

Projective imaging of high-energy nuclei through coherent exclusive vector meson production in electron-ion collisions

Maci Kesler¹, Ashik Ikbal Sheikh¹, Rongrong Ma², Zhoudunming Tu², Thomas Ullrich², Zhangbu Xu^{1,2}

¹Department of Physics, Kent State University, Kent, OH 44240 USA and

²Brookhaven National Laboratory, Upton, New York 11973 USA

(Dated: April 1, 2025)

One of the major goals of the Electron-Ion Collider (EIC) is to study the distributions of gluons inside nuclei at high energy. A principal measurement is the coherent exclusive vector meson (VM) production in diffractive electron-nucleus collisions, where the gluon spatial distribution inside the nucleus can be obtained through a Fourier transform of the squared nuclear momentum transfer ($|t|$) distribution during the process. However, the $|t|$ distribution is one of the most challenging measurements at the EIC. This research aims to overcome the two main obstacles of the $|t|$ measurement: limited precision in measuring $|t|$ arising from the momentum resolution of the outgoing electron and the overwhelming incoherent background. We demonstrate that by measuring the projected $|t|$ distribution along the direction perpendicular to the electron scattering plane, the effect of the outgoing electron's momentum resolution can be effectively mitigated, and the diffractive pattern is largely restored. Furthermore, we propose to measure the angular distribution of the VM's decay daughters to statistically remove the incoherent background.

I. INTRODUCTION

The Electron-Ion Collider (EIC), to be built at the Brookhaven National Laboratory (BNL) in the US, has been designated as a high-priority construction project over the coming decade to study the fundamental properties of the Quantum ChromoDynamics (QCD) [1]. A core mission of the EIC is to image the gluon spatial distributions in nuclei and understand the underlying dynamics, such as the phenomenon of gluon saturation [2]. A mission-critical measurement is the coherent exclusive vector meson (VM) production, such as ρ , ω , ϕ , and J/ψ , etc, in diffractive electron-nucleus ($e+A$) collisions.

A diffractive $e+A$ collision is depicted in Fig. 1. An electron comes in, emits a virtual photon (γ^*) with virtuality Q^2 , and scatters away. The virtual photon fluctuates into a quark-antiquark pair, interacts with the nucleus through an exchange of a Pomeron (blue blob), and

emerges as a VM without any other final-state particles produced in the process. The squared four-momentum transfer of the nucleus is denoted as t , and W^2 is the squared invariant mass of the γ^* -nucleus system. The spatial distribution of gluons inside the nucleus can be extracted through a Fourier transformation of the $|t|$ distribution in coherent events where the incoming nucleus remains intact.

At the EIC, exclusive VM production in diffractive events constitutes a significant fraction of the $e+A$ collision cross section. Compared to photonuclear production of VMs in ultraperipheral heavy-ion collisions [4? , 5], which can also be used to study gluon distribution in a heavy nucleus but is limited to the phase space of $Q^2 \sim 0$, measuring the VM production over a large Q^2 range down to low x (fraction of the nucleon's longitudinal momentum carried by a gluon), which can only be realized by the EIC [1], will gain a more comprehensive understanding of the gluon distributions in nuclei.

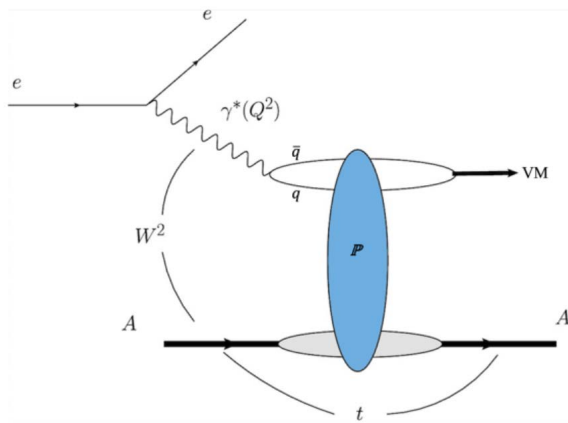


FIG. 1. Exclusive VM production in a coherent diffractive $e+A$ collision [3].

However, measuring the $|t|$ distribution for coherent VM production in $e+A$ collisions encounters two critical challenges: (i) limited precision in measuring $|t|$ arising mainly from the momentum resolution of the outgoing electron, and (ii) the overwhelming incoherent background when the nucleus breaks up. In this work, we exploit the $|t|$ distribution projected along the normal direction of the electron scattering plane to alleviate the effect of electron momentum resolution and to a large extent restore the expected features of the $|t|$ distribution for coherent events. We also propose to utilize transversely polarized electron beams and take advantage of the unique angular distribution of the daughter particles from VM decays to eliminate the contribution of incoherent production on an ensemble basis.

II. METHOD

For a heavy nucleus, the $|t|$ distribution is given by a form factor, whose analytic form can be obtained through the convolution of the Yukawa potential with the Woods-Saxon distribution approximated as a hard sphere potential [6, 7]:

$$F(t) = \frac{4\pi\rho_0}{Aq^3} [\sin(tR) - tR \cos(tR)] \left(\frac{1}{1 + a^2 t^2} \right), \quad (1)$$

where $t = q^2$, ρ_0 is the nuclear density at the center of the nucleus, A is the atomic mass number, R is the nuclear radius, and the range of the Yukawa potential is given by $a = 0.7$ fm.

A. Current Challenges

The challenges of measuring the $|t|$ distribution, based on the current detector design for the EIC [2], are illustrated in Fig. 2. The black solid curve shows the typical $|t|$ distribution for coherently produced J/ψ mesons in $e+A$ collisions based on Eq. 1. A distinct structure of peaks and valleys is seen, where the positions of the valleys or minima are determined by the gluon spatial distribution in the scattered nucleus, while the magnitude of the distribution is sensitive to the saturation effect. The expected $|t|$ distribution after considering the detector resolution, especially the outgoing electron's momentum resolution, is shown as blue circles, where the structure of peaks and valleys is largely washed out, making it extremely difficult for extracting the spatial gluon distribution. In addition to coherently produced VMs, there are also VMs produced in incoherent diffractive events shown as the black squares, whose yields dominate over coherent production in most of the interested $|t|$ range. While the incoherent production is of interest on its own, it acts as an overwhelming background for measuring coherent production. Current detector design can significantly suppress the incoherent production by tagging nuclear fragments on an event-by-event basis, as illustrated by the red diamonds, but we are still only able to resolve the first minimum. To resolve the second and third minima, another order of magnitude suppression is needed, which is extremely challenging, if not impossible, with the current detector design.

B. Projective Technique

To overcome the challenge of insufficient experimental precision in resolving the diffractive pattern of the coherent $|t|$ distribution, we propose to measure the projection of $|t|$ along the normal direction of the electron scattering plane. Figure 3 shows another diagram for a coherent exclusive VM production event ($e + A \rightarrow e' +$

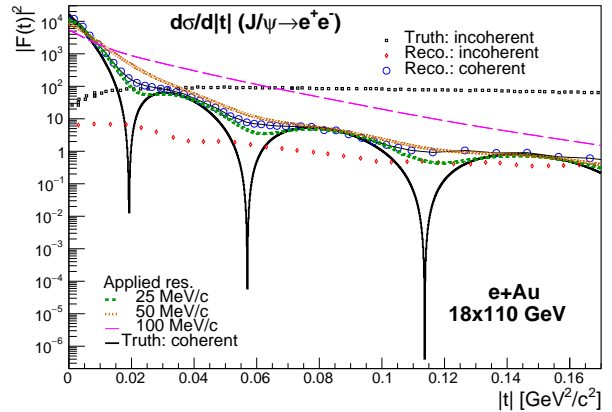


FIG. 2. $|t|$ distributions for coherent and incoherent exclusive J/ψ production in $e+A$ collisions. The coherent distribution, based on Eq. 1, is shown as the black solid curve. This is the maximum possible diffraction pattern one can achieve. The blue circles represent the expected $|t|$ distribution one can measure based on the EIC detector design [2]. Distributions of incoherent J/ψ production before (black squares) and after (red diamonds) being suppressed with current EIC detector design are also displayed. The green dashed, orange dotted and magenta long dashed curves show the coherent $|t|$ distributions after smearing the theoretical prediction (black solid curve) with a resolution of 25, 50 and 100 MeV/c, respectively.

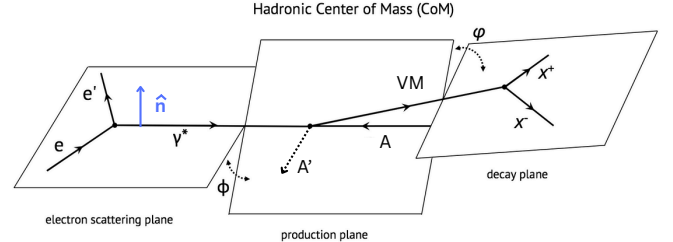


FIG. 3. Coherent exclusive VM production in an $e+A$ collision [6]. The normal direction (\hat{n}) to the electron scattering plane is shown as the blue vertical arrow.

$A' + VM$), where e and e' denote incoming and outgoing electrons, γ^* represents the emitted virtual photon, A and A' are the incoming and outgoing nuclei, and VM indicates the produced VM that decays into X^+ and X^- [6]. The blue vertical arrow points along the normal direction (\hat{n}) of the electron scattering plane, spanned by the momenta of incoming and outgoing electrons. We can then decompose t as

$$t = t_\perp + t_\parallel, \quad (2)$$

where $t_\perp = t_x + t_y$ and t_\parallel are transverse and longitudinal components. t_\parallel lies along the z direction, defined as the virtual photon's travel direction within the electron scattering plane. t_x and t_y are the components along x and y

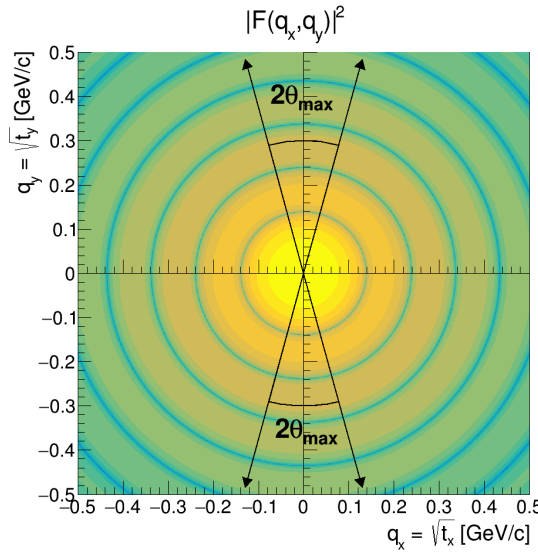


FIG. 4. Distribution of the form factor from Eq. 1 as a function of (q_x, q_y) .

directions, where the y direction is parallel to \hat{n} and the x direction is within the electron scattering plane and perpendicular to z . t_{\parallel} is determined by the VM mass and longitudinal momentum conservation, and is neglected in this work as usually $t_{\parallel} \ll t_{\perp}$ for high-energy nuclei [6]. We further define:

$$t_{\perp} = q_{\perp}^2 = q_x^2 + q_y^2, \quad (3)$$

$$q_x = q_{\perp} \sin(\theta), \quad q_y = q_{\perp} \cos(\theta), \quad (4)$$

where θ is the angle between \mathbf{q}_{\perp} and q_y in the $x - y$ plane. Due to momentum conservation, the $q_{x,y}$ are the VM momentum components along those axes. The form factor for coherent VM production (1) as a function q_x and q_y is shown in Fig. 4, where the diffractive pattern of peaks and valleys show up as concentric circles. We can now cut a wedge of angle ($\theta < \theta_{\max}$) to obtain the projected $|t|$ distribution along the \hat{n} or y direction:

$$|F(t)|^2 \rightarrow \int_0^{\theta_{\max}} |F'(t, \theta)|^2 d\theta = |F_{\hat{n}}(t)|^2. \quad (5)$$

Consequently, when θ_{\max} is small, most of the q_x component, and thus the outgoing electron's momentum resolution, is eliminated. Only the electrons' momentum directions before and after scattering are needed to determine the \hat{n} direction, which can be measured with much better precision than their momenta.

To overcome the challenge of the coherent signal being swamped by the incoherent background, we propose to exploit the decay pattern of the VM with respect to \hat{n} to accurately determine the fraction of coherently produced VMs in collisions of transversely polarized electron beams, *i.e.*, the electron spin is perpendicular to its momentum.

In coherent events where the incoming electron flips its spin after scattering, the spin of the emitted virtual photon will align with the spin of the incoming electron since the exchanged Pomeron has 0 spin, and finally transfers to the produced VM. In other words, the spin of the VM will align with \hat{n} in such events. We can then project the momentum of the VM's decay daughter onto the VM's spin direction, \hat{s} (*i.e.*, \hat{n}), a $\cos(2\phi)$ modulation is expected [8], where ϕ denotes the angle between the momentum of the decay daughter in the VM's rest frame and \hat{n} . On the other hand, if the spin of the incoming electron does not flip during scattering, there will be no preferred direction for the spin of the virtual photon or the VM, and a flat ϕ distribution is expected. Similarly, in an incoherent event where the nucleus breaks up, the spin of the VM is expected to be random with respect to \hat{n} , and therefore no $\cos(2\phi)$ modulation should be observed either. Consequently, the fraction of coherent events where the incoming electron flips its spin is equal to $\langle \cos(2\phi) \rangle$. Here, the average runs over all exclusive VM events. If we assume that the probability for the incoming electron to flip its spin is C , which is expected to be independent of $|t|$ since they are causally disconnected, the fraction of total coherent events will be $\langle \cos(2\phi) \rangle / C$ in the event sample. By measuring such a fraction in each $|t|$ bin, one can obtain the $|t|$ distribution for the coherent VM production on an ensemble basis. As a by-product, one can also obtain the incoherent VM cross section as a function of $|t|$, from which fluctuations in the gluon density can be studied.

This projective imaging technique takes advantage of several features of diffractive processes:

- The interaction of the virtual photon and the Pomeron as shown in Fig. 1 is isotropic in the t_{\perp} plane because the exchanged Pomeron is spin 0. This means that selection on a specific wedge of the t_{\perp} plane does not lose any information. Measurements of higher-order interactions may be affected by the wedge cut and should be taken into account in future work [9, 10].
- The $|t|$ resolution is dominated by the energy and momentum measurements of the scattered electrons, while their angular resolution is negligible. Therefore, a wedge selection perpendicular to the electron scattering plane minimizes the impact of the detector resolution.
- The fact that the Pomeron has 0 spin allows the transfer of the electron polarization to the emitted photon and finally to the coherently produced VM, with the spin direction fully determined. Due to the conservation of angular momentum, the decay pattern of the VM can therefore be utilized to distinguish coherent from incoherent production.

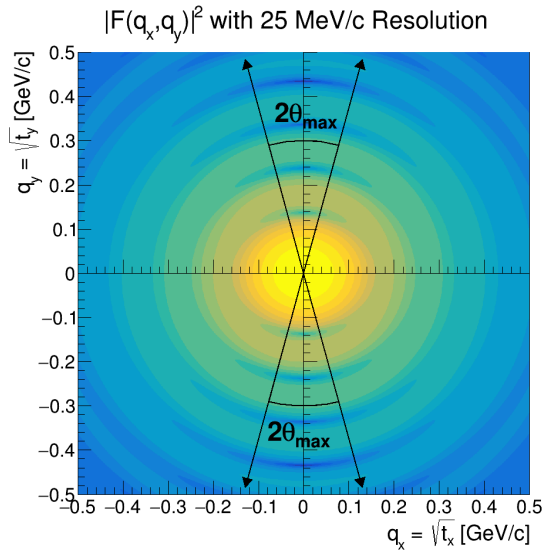


FIG. 5. Distribution of the form factor from Eq. 1 as a function of (q_x, q_y) , with 25 MeV/c resolution added to the q_x axis. A wedge cut of $\theta_{\max} = \pi/12$ from the q_y axis is indicated by arrows.

III. RESULTS

In this section, we focus on demonstrating that one is able to alleviate the limited $|t|$ resolution and largely restore the diffractive pattern for coherent VM production by measuring the projective $|t|$ distribution using a wedge cut. The statistical separation of coherent and incoherent production through decay patterns is less intricate and will be further explored in future work.

To mimic the detector resolution, we smear the coherent $|t|$ distribution from its analytic form, *i.e.*, black solid curve in Fig. 2, with three constant resolution values, 25, 50 and 100 MeV/c, independent of $|t|$. This is done by convoluting Eq. 1 with a Gaussian distribution to smear the q_x component. Resulting $|t|$ distributions are shown in Fig. 2, where one can see the designed detector resolution (open circles) lies between 25 to 50 MeV/c of resolution. For the following results, the 25 MeV/c resolution is used.

The smeared $|F(t = q^2)|^2$ distribution as a function of q_x and q_y is shown in Fig. 5. Compared to Fig. 4 where no detector resolution is included, the distribution becomes more elliptical along the q_x axis, a direct consequence of the electron momentum resolution. The projected $|t|$ distribution ($|F_{\hat{n}}(t)|^2$) is obtained by applying a wedge cut of $\theta_{\max} = \pi/12$, indicated by black arrows in Fig. 5, and shown in Fig. 6 as the dashed magenta curve. Compared to the case of no wedge cut or equivalently $\theta_{\max} = \pi/2$ (blue long-dashed line in Fig. 6), where the diffractive pattern is largely washed out, one can see a clear structure of peaks and valleys in the projected $|t|$ distribution for a wedge cut of $\theta_{\max} = \pi/12$.

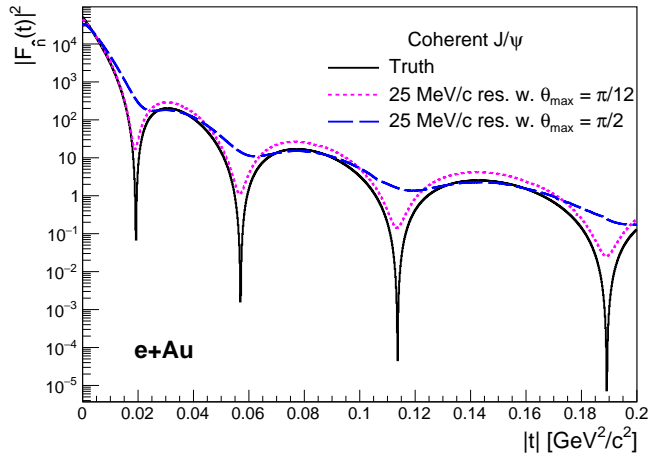


FIG. 6. Projected $|t|$ distribution with a wedge cut of $\theta_{\max} = \pi/12$ for coherent VM production. It is compared to the theoretical expectation of the full $|t|$ distribution as well as that with detector resolution but no wedge cut (*i.e.*, $\theta_{\max} = \pi/2$). Both curves have been normalized by a factor of $A / \int |F_{\hat{n}}(t)|^2$ where $A = 197$ for gold and $|F_{\hat{n}}(t)|^2$ is determined by the angle θ_{\max} .

Such a significant improvement in resolving the diffractive pattern is critical for utilizing the $|t|$ measurement for imaging the gluon spatial distribution inside nuclei. The price one pays with the wedge cut is the loss of statistics. For example, about 83% of coherent VM events are thrown away with the $\theta_{\max} = \pi/12$ wedge cut for the 25 MeV/c resolution. The optimal wedge selection should be determined experimentally based on the detector resolution and available statistics. For completeness, the analytical distribution of the form factor is also in Fig. 6 as the black solid curve. As expected, the diffractive pattern is more distinct compared to the case with detector resolution and a wedge cut.

IV. SUMMARY AND OUTLOOK

In summary, we developed a unique approach to overcome the challenges of incoherent background and limited detector resolution in utilizing coherent VM production for imaging the gluon spatial distribution in the nucleus at the future EIC. Specifically, the incoherent background can be separated from coherent VM production in collisions of transversely polarized electron beams by exploiting the angular distribution of decay daughters from VM. Moreover, the projected $|t|$ distribution perpendicular to the electron scattering plane can be used to avoid the effect of limited precision in measuring the outgoing electron's momentum with the current EIC detector design. By applying a wedge cut in the transverse $|t|$ plane, the theoretically-predicted diffractive pattern for coherent VM production is largely restored, from which the

gluon distribution in the nucleus and its dynamics can be inferred.

In future work, we will implement this approach into the simulation of the ePIC detector, the baseline detector for the EIC. We will determine the best wedge cut based on the projected EIC luminosity and realistic detector resolution, including its $|t|$ dependence, and study the residual effect from energy and angular resolutions of outgoing electrons. An unfolding procedure will be explored to account for the detector resolution in measuring the projected $|t|$ distribution. This work will open

the door for the mission-critical measurement of exclusive VM production in studying gluon distributions, and enhance the scientific output of the EIC project.

ACKNOWLEDGMENTS

This research is supported by the US Department of Energy, Office of Nuclear Physics (DOE NP), under contract Nos. DE-FG02-89ER40531, DE-SC0012704.

[1] R. Abdul Khalek *et al.*, Science Requirements and Detector Concepts for the Electron-Ion Collider: EIC Yellow Report, *Nucl. Phys. A* **1026**, 122447 (2022), arXiv:2103.05419 [physics.ins-det].

[2] J. Adam *et al.* (ATHENA), ATHENA detector proposal — a totally hermetic electron nucleus apparatus proposed for IP6 at the Electron-Ion Collider, *JINST* **17** (10), P10019, arXiv:2210.09048 [physics.ins-det].

[3] M. Krelina, V. P. Goncalves, and J. Cepila, Coherent and incoherent vector meson electroproduction in the future electron-ion colliders: the hot-spot predictions, *Nucl. Phys. A* **989**, 187 (2019), arXiv:1905.06759 [hep-ph].

[4] S. Acharya *et al.* (ALICE), Coherent photoproduction of ρ^0 vector mesons in ultra-peripheral Pb-Pb collisions at $\sqrt{s_{NN}} = 5.02$ TeV, *JHEP* **06**, 035, arXiv:2002.10897 [nucl-ex].

[5] L. Adamczyk *et al.* (STAR), Coherent diffractive photoproduction of ρ^0 mesons on gold nuclei at 200 GeV/nucleon-pair at the Relativistic Heavy Ion Collider, *Phys. Rev. C* **96**, 054904 (2017), arXiv:1702.07705 [nucl-ex].

[6] M. Lomnitz and S. Klein, Exclusive vector meson production at an electron-ion collider, *Phys. Rev. C* **99**, 015203 (2019), arXiv:1803.06420 [nucl-ex].

[7] T. Toll and T. Ullrich, Exclusive diffractive processes in electron-ion collisions, *Phys. Rev. C* **87**, 024913 (2013), arXiv:1211.3048 [hep-ph].

[8] M. Abdallah *et al.* (STAR), Tomography of ultrarelativistic nuclei with polarized photon-gluon collisions, *Sci. Adv.* **9**, eabq3903 (2023), arXiv:2204.01625 [nucl-ex].

[9] J. D. Brandenburg, H. Duan, Z. Tu, R. Venugopalan, and Z. Xu, Entanglement enabled intensity interferometry in ultrarelativistic ultraperipheral nuclear collisions, *Phys. Rev. Res.* **7**, 013131 (2025), arXiv:2407.15945 [hep-ph].

[10] Y. Hagiwara, C. Zhang, J. Zhou, and Y.-j. Zhou, Probing the gluon tomography in photoproduction of dipion, *Phys. Rev. D* **104**, 094021 (2021), arXiv:2106.13466 [hep-ph].

[11] S. Klein and J. Nystrand, Exclusive vector meson production in relativistic heavy ion collisions, *Phys. Rev. C* **60**, 014903 (1999), arXiv:hep-ph/9902259.

[12] A. Accardi *et al.*, Electron Ion Collider: The Next QCD Frontier: Understanding the glue that binds us all, *Eur. Phys. J. A* **52**, 268 (2016), arXiv:1212.1701 [nucl-ex].

[13] J. K. Adkins *et al.*, Design of the ECCE detector for the Electron Ion Collider, *Nucl. Instrum. Meth. A* **1073**, 170240 (2025), arXiv:2209.02580 [physics.ins-det].

[14] A. Caldwell and H. Kowalski, Investigating the gluonic structure of nuclei via J/psi scattering, *Phys. Rev. C* **81**, 025203 (2010).

[15] National Academies of Sciences, Engineering, and Medicine, *An Assessment of U.S.-Based Electron-Ion Collider Science* (The National Academies Press, Washington, DC, 2018).

[16] H. B. Prosper and L. Lyons, eds., *CERN Yellow Reports: Conference Proceedings* (CERN, Geneva, 2011).

[17] EIC User Group and ePIC Collaboration: <https://eic.github.io/>, (2023).